Ceramics International 47 (2021) 22147–22154

Contents lists available at ScienceDirect

Ceramics International

journal homepage: www.elsevier.com/locate/ceramint

Eco-friendly $Bi(Ni_{2/5}Ti_{2/5}Fe_{1/5})O_3$ nanoceramics: Synthesis, dielectric and impedance studies

Nitin Kumar [a,*], Alok Shukla [a], Nripesh Kumar [a], Ravi Agarwal [b], R.N.P. Choudhary [c]

[a] Department of Physics, National Institute of Technology Mizoram, Aizawl, 796012, India
[b] Centre for Converging Technologies, University of Rajasthan, Jaipur, 302004, Rajasthan, India
[c] Multifunctional Materials Research Laboratory, Department of Physics, ITER, Siksha O Anusandhan University, Bhubaneswar, 751030, Odisha, India

ARTICLE INFO

Keywords:
Eco-friendly nanoceramic
X-ray diffraction
Dielectric properties
Crystal structure
Impedance spectroscopy

ABSTRACT

This investigation involves the synthesis and study of dielectric, structural and impedance properties of polycrystalline $Bi(Ni_{2/5}Ti_{2/5}Fe_{1/5})O_3$ (symbolized as BNTF) nano-ceramic. The BNTF polycrystalline sample was fabricated through the use of a conventional solid-state reaction route. X-ray structural examination reveals that the parent compound (i.e., $BiFeO_3$) crystallizes in the rhombohedral structure (space group-R3c) while that the BNTF compound crystallizes in orthorhombic symmetry. The substitution of $NiTiO_3$ into $BiFeO_3$ enhances various properties and reduces electrical leakage current. The average crystallite size is calculated to be 29 nm. The room temperature textures and surface morphologies of the specimen were verified by field-emission scanning electron microscope, and show uniform grains distribution on sample surfaces. Dielectric parameters (constant and tangent-loss) and impedance spectroscopy parameters of $NiTiO_3$ modified $BiFeO_3$ compound were investigated over a wide temperature range (25–500 °C) at different frequency (25 kHz-500 kHz), which offers several interesting features of BNTF material suitable for further device applications.

1. Introduction

Over the last few decades, the subject of multiferroics has been considered as the hottest theme/topic of materials science and solid-state physics. The occurrence of two or more ferroic order parameters simultaneously in single-phase material is referred as multiferroics. These materials have attracted much more attention because of their possible applications in numerous devices (i.e., spintronic, memory storage, ultrafast optoelectronic devices, sensors, magnetically modulated transducers etc.) [1–5]. The existence of order parameters in multiferroics provides possibilities of new features in novel multifunctional devices. The recent activities on the multiferroics research offer novel multifunctional materials and discoveries that have been verified by both theoretical and experimental approaches. These few sets of materials have shown both ferroelectric and magnetic polarizations [6]. Among numerous multiferroic material systems, $BiFeO_3$ is the most studied compound so far because of the coupling between magnetic and ferroelectric order in it at the room temperature. At room temperature, the crystal symmetry of bismuth ferrite polar phase is best defined in rhombohedral structure (perovskite) along with R3c space group. In $BiFeO_3$, the occurrence of ferromagnetic properties is due to the existence of Fe^{+3} ions, and the ferroelectric properties are due to the $6s^2$ electrons (in the form of lone paired) of Bi^{+3} [7,8]. The major drawbacks of $BiFeO_3$ (BFO) are the large leakage density, much higher tangent loss and structural distortion that affect its dielectric, resistive and ferroelectric behaviours. The large leakage current density is accredited to oxidation-reduction of iron-ions generating oxygen positions for the charge compensation [9,10].

Though few progressive development techniques have been tried to develop the compounds having multiferroic features with a large coupling coefficient, the subject of an appropriate process is to combine several types of process. In addition, the nickel titanate ($NiTiO_3$) displayed rhombohedral symmetry in which nickel and titanium atoms are desired to form an octahedral coordination system with irregular cation layers solely employed through either nickel or titanium [11,12]. To eliminate the said inherent problems of BFO, this work has been designed to produce eco-friendly complex $Bi(Ni_{2/5}Ti_{2/5}Fe_{1/5})O_3$ multiferroic material. Similar theme of the work is not reported in the literatures [13,14].

This work reports on the synthesis and characterization (structural, dielectric, impedance and multiferroics characteristics) of nickel and titanium modified bismuth ferrites (i.e., $Bi(Ni_{2/5}Ti_{2/5}Fe_{1/5})O_3$)

* Corresponding author.
E-mail address: nitinphysicskushawaha@gmail.com (N. Kumar).

https://doi.org/10.1016/j.ceramint.2021.04.237
Received 18 January 2021; Received in revised form 18 April 2021; Accepted 23 April 2021
Available online 3 May 2021

ceramics.

2. Materials, method and measurements

An eco-friendly (Pb-free) $Bi(Ni_{2/5}Ti_{2/5}Fe_{1/5})O_3$ (BNTF) nanoceramic was prepared by using a conventional solid-state reaction route [15,16]. All chemicals (carbonate and oxides) of analytical grade procured from the Merck were used. First, these ingredients, $(BiO)_2CO_3.H_2O$ (bismuth carbonate), NiO (nickel oxide), Fe_2O_3 (iron oxide) and TiO_2 (titanium dioxide), were thoroughly mixed in a suitable stoichiometric ratio in mortar and pestle in air atmosphere for 10 h, and then in wet medium (methanol) for 10 h. The fine homogeneous powder of ingredients was calcined at an optimized temperature of 750 °C for 8 h. The single-phase formation and basic structural symmetry were tested using X-ray diffractometer (Japan-Rigaku: Powder) with the specific (CuKα; λ = 1.5405 Å) radiation in a wide range of Bragg angles ($20° \leq 2\theta \leq 60°$) at slow scan speed. The surface morphology of prepared specimen was recorded through the field emission scanning electron microscope (Carl Zeiss: EVOHD-15). The calcined powder of the desired compound was used to form circular-shaped pellets (thickness = ~1.5 mm; diameter = 8 mm) by a hydraulic KBr press (pressure = 4.5×10^6 N/m^2). As-prepared BNTF pellets were sintered at 800 °C (optimized temperature) for 8 h in normal air medium. Before their electrical measurements, the sintered pellet was ground through a fine paper (emery) to make the pellet surface smooth and parallel, and then both surfaces of pellet were polished with the conducting paste (silver). The capacitance (C_p in parallel combination), phase angle (θ), impedance (Z) and tangent loss (tan δ) were recorded in a wide temperature range (25–500 °C) at a different frequency (10 kHz–500 kHz) by means of computer-interfaced phase-sensitive multi-meter (PSM:1735, UK-Newton N4L) with the laboratory-designed sample holder. The detailed description of the synthesis process is summarized in Fig. 1.

2.1. P-E loop tracer

The ferroelectricity (FE) is a subclass of pyroelectricity. The FE hysteresis loop directly sustains ferroelectric nature in the studied material. Additionally, the polarization vs. electric field hysteresis loop in the case of ferroelectrics are analogous to those of magnetic hysteresis loop (magnetization versus magnetic field). Ferroelectric materials exhibit polarization vectors that could be oriented into two reverse directions. The displacement reduces the symmetry of the material/crystal spontaneously also thermodynamically stable states can be exchanged from one to another direction by using an external electric field. Commonly, the ferroelectric materials contain domains (the regions where several unit cells holding displaced ions in a similar direction) which has an effect of polarization under electric field.

The poling process in which, the oriented electric dipoles are aligned in an identified direction. The procedure of poling is to shift opposite domains under the Tc (transition temperature) with greater electric fields than the coercive field. For numerous compounds having higher coercivity values allow poling only close to Tc, but in some of the compounds, electrical poling might succeed through cooling of the compounds from their paraelectric to ferroelectric phase in an electric field (applied) parallel with polar crystallographic axis in the influence of the constant electric field. In the present study, the polarization versus electric field (P-E hysteresis loops) as-studied sample at various fields have been attained using the hysteresis loop tracer (Marine India). Fig. 2 represents the schematic setup of ferroelectric loop tester.

2.2. M − H loop tracer

The magnetic field dependence of magnetization has been studied at normal/room temperature (298 K) by means of a physical property measurement system and superconducting quantum interference device magnetometer. It is a great deal of evidence about the magnetic characteristics of material could obtain through the hysteresis loop. A hysteresis loop diagram displays the relationship between the induced magnetic field (H) and magnetization (M). It is denoted as the M − H hysteresis loop. By the hysteresis loop spectrum, a number of primary magnetic characteristics of material could be determined as such manner retentivity, coercive field, permeability, residual magnetism as

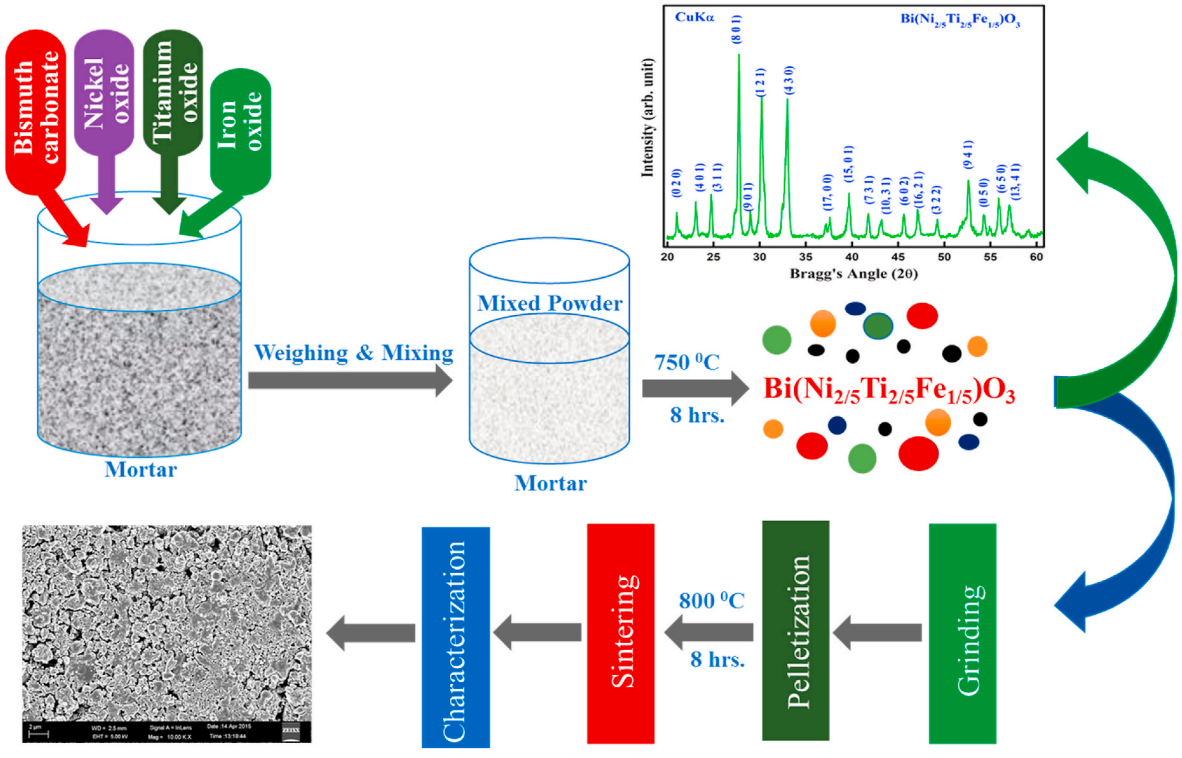

Fig. 1. Schematic syntheses process of $Bi(Ni_{2/5}Ti_{2/5}Fe_{1/5})O_3$ nanoceramic by the solid-state reaction route.

Fig. 2. Representation of P-E loop tracer setup.

well as the reluctance.

The experimental technique of the vibrating sample magnetometer (VSM), was initially developed by the Foner. It is effective technique for the analysis of higher magnetic field and low-temperature examines of correlated electron systems because of simplicity as well as high sensitivity. The superconducting quantum interference device detects and measures the magnetic parameters of the sample. The magnetic hysteresis of nickel and titanium co-substituted BFO ceramics have been measured using vibrating sample magnetometer (Quantum Design; Fig. 3) at room temperature.

Fig. 3. Representation of VSM (Quantum Design).

3. Results and discussion

3.1. The analysis of structural symmetry and their microstructure

The X-ray diffraction (XRD) technique is more effective and extensively used method for materials characterization. It could detect the chemical compounds from their crystal structure. Therefore, the specimen that having different compounds but has a similar composition could be identified by this method. Fig.4 depicts a powder XRD pattern of $Bi(Ni_{2/5}Ti_{2/5}Fe_{1/5})O_3$ (BNTF) at room temperature. The sharp peaks of the pattern confirm good crystallinity of the compound. The existence of most prominent peaks of the patterns is related to perovskite symmetry, but not similar those of the ingredients. As a result, the BNTF crystal system was confirmed with the existence of a new phase of the system. The XRD configuration of prepared BNTF system also displayed higher angle splitting, hereafter the peak distribution trend confirmed the presence of orthorhombic symmetry. The tolerance factor for Ni/Ti doped ABO_3 perovskite like-$BiFeO_3$ structure is defined as [15,17],

$$t = \frac{(r_A + r_O)}{\sqrt{2}.(r_B + r_O)}$$

Here $\langle r_A \rangle$ and $\langle r_B \rangle$ represents calculated average ionic radii of the bismuth (at the A-site) and nickel, titanium, iron (at the B-site) cations and r_o represents ionic radii of oxygen atom respectively. However, the tolerance factor mainly belongs to measure the structural stability of the perovskite structure. The calculated tolerance factor value of BNTF ceramic is 0.85, which confirms a deviation from ideal perovskite (t = 1) structure.

Furthermore, the standard 'POWD' software has been applied to index all peaks in optimized crystal symmetry [18]. The subject of the better comparison between the experimental and measured d values (d = inter planar spacing distance) [$\sum\Delta d = d_{experimental} - d_{measured} =$ minimum]; the system was established to fit in orthorhombic symmetry. The least-squares refined cell parameters are; a = 40.4631 Å, b = 8.2439 Å, c = 4.1483 Å (with ±0·002 as minimum standard deviation). By using a strong reflection peak (8 0 1) of the XRD pattern, the measured crystallite dimension was found to be 36 nm from reflections broadening by means of Scherrer's equation [defined as $D_{XRD} = K.\lambda/\beta.cos\theta$] [19]. In this relation, the constant term K (=0.89) is subjected to the shape of crystallite size, λ is subjected to the wavelength of radiation (Cu K_α; 1.5406 Å), β = full width at half maximum of intensity vs. 2θ scheme and the term θ is subjected to Bragg's diffraction angle. From the calculations, the average crystallite size of as-synthesized BNTF ceramic is 29 nm which is comparable to that of our previous reported value for BNTF and BCTF ceramic [13,14,20,21]. The detailed information about their d-spacing values, relative intensities and plane position has displayed in Table 1. Additionally, few results showing the similar structural symmetry with the (Co, Ni, Cd with Ti) addition/co-substituted bismuth ferrite have been summarized in Table 2.

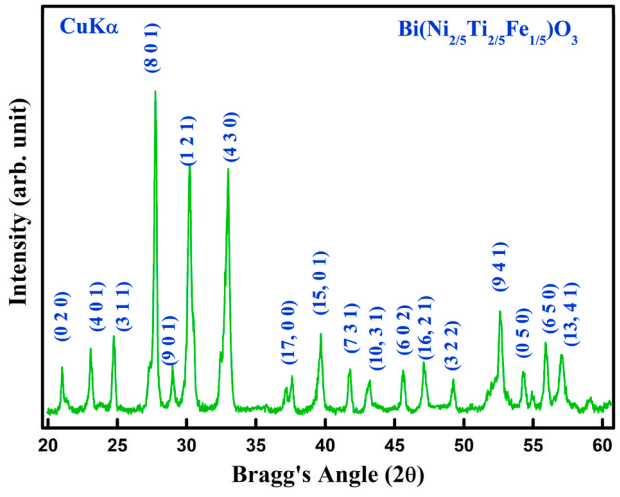

Fig. 4. Powder X-ray diffraction pattern of $Bi(Ni_{2/5}Ti_{2/5}Fe_{1/5})O_3$ nanoceramic at room temperature.

The field-emission scanning electron (symbolized as FE-SEM) is the best multipurpose instrument for the depth examination and analysis of the microstructural morphology of solid ceramic specimens. Fig.5 shows the FE-SEM image of BNTF sintered pellet at room temperature. The image confirms that the grains are highly packed with a lower degree of voids, and are homogeneously scattered through the sample surface. The observed grains are in the form of different sizes and shapes, clearly indicating the presence of polycrystalline microstructure behaviour. The grains are of partially equal sizes, however, showing different grain restrictions. The average grains dimension was calculated and found in the range of 120–300 nm. As the crystallites size is not similar to their grain size, results in the difference in their structural parameters.

3.2. The analysis of dielectric studies

Fig. 6 (a, b) demonstrates relative dielectric constant (ε_r) and corresponding tangent loss (tan δ) variation plot at a different frequency (25, 50, 100 and 500 kHz) and temperature (room temperature to 500 °C). The figure depicts the dielectric dispersion curves showing strong frequency and temperature dependent relation of both dielectric parameters (tan δ) and (ε_r). At all frequencies, the magnitude of relative dielectric constant value increases linearly with the increase in temperature nonetheless both dielectric parameters (ε_r and tan δ) value decrease on rising frequency, that is the general features of dielectrics [4,22]. This type of variation occurred in dielectric constant spectrum might be due to the dissimilar kinds of polarization (like dipolar, ionic, dipolar and so on) and space charge occurred in compounds at a higher frequency. The subject of the several sets of polarization mechanisms, a short-range displacement can happen and lead the entire polarization of the compound, and hereafter to its dielectric permittivity [23]. The magnitude of the dielectric constant values increases on increasing temperature, which is because of the existence of electron-phonon relations.

The value of dielectric constant at a particular frequency of 25 kHz at room temperature and 500 °C are 256 and 627 correspondingly. The increment of ε_r value could be attributed to the thermally activated space charge transport. Additionally, the calculated values of dielectric loss at a particular frequency of 25 kHz at room temperature and 500 °C

Table 1
Comparison of observed and calculated d-values of their major reflections for $Bi(Ni_{2/5}Ti_{2/5}Fe_{1/5})O_3$ at room temperature. Compound: $Bi(Ni_{2/5}Ti_{2/5}Fe_{1/5})O_3$ Symmetry: Orthorhombic Phase.

Peak	2θ	d_{obs}(Å)	d_{cal}(Å)	I/I_o	h	k	L
1	21.02	4.2227	4.2219	15	0	2	0
2	23.08	3.8502	3.8485	21	4	0	1
3	24.74	3.5955	3.5966	25	3	1	1
4	27.74	3.2131	3.2178	100	8	0	1
5	28.98	3.0784	3.0841	16	9	0	2
6	30.22	2.9549	2.9548	77	1	2	1
7	33.00	2.7120	2.7125	76	4	3	0
8	37.60	2.3901	2.3908	13	17	0	0
9	39.68	2.2695	2.2701	25	15	0	1
10	41.78	2.1601	2.1631	14	7	3	1
11	44.78	2.0221	2.0220	10	10	3	1
12	45.60	1.9977	1.9876	14	6	0	2
13	47.10	1.9278	1.9284	20	16	2	1
14	49.24	1.8489	1.8478	11	3	2	2
15	52.60	1.7384	1.7374	32	9	4	1
16	54.26	1.6891	1.6888	14	0	5	0
17	55.88	1.6439	1.6453	23	6	5	0
18	57.02	1.6136	1.6126	19	13	4	1

Table 2
Structural symmetry for (Co, Ni, Cd with Ti) addition/co-substituted bismuth ferrite.

S. No.	Compounds Name	XRD Symmetry	Average crystallite size	Reference
1.	Bi $(Co_{0.40}Ti_{0.40}Fe_{0.20})O_3$	Orthorhombic structure	30 nm	[5]
2.	Bi $(Ni_{0.40}Ti_{0.40}Fe_{0.20})O_3$	Orthorhombic structure	36 nm	[13]
3.	$Bi(Cd_{1/4}Ti_{1/4}Fe_{1/2})O_3$	Orthorhombic structure	30 nm	[14]
4.	Bi $(Cd_{0.45}Ti_{0.45}Fe_{0.10})O_3$	Orthorhombic structure	30 nm	[20]
5.	Bi $(Co_{0.45}Ti_{0.45}Fe_{0.10})O_3$	Orthorhombic structure	30 nm	[21]
6.	$Bi(Ni_{2/5}Ti_{2/5}Fe_{1/5})O_3$	Orthorhombic structure	29 nm	Present paper

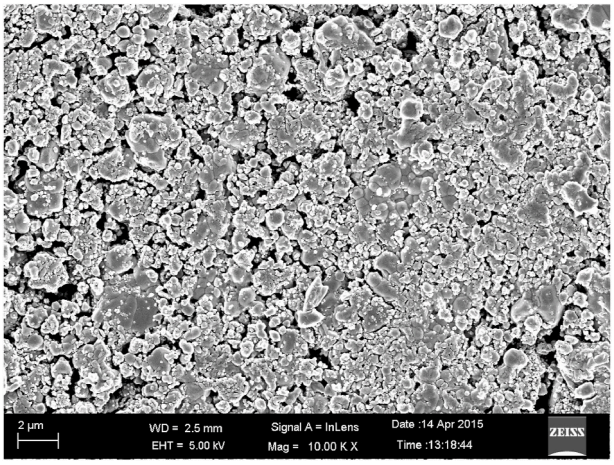

Fig. 5. FE-SEM micrograph of $Bi(Ni_{2/5}Ti_{2/5}Fe_{1/5})O_3$ nanoceramic at room temperature.

are 0.03 and 1.92 correspondingly. Within the limitation of experimental setup on material characteristics, the phase transition could not be detected in the temperature range of (25 ^{0}C-500 °C). The trend in tan δ variation with temperature is similar to that of ε_r (the magnitude of tan δ value gradually rises on increasing temperature) values. In general, the high value of tan δ in the low-frequency zone and high temperatures is just because of the iron-containing materials that reduce quickly with the increase in frequency. A similar temperature variation of the dielectric loss has been reported earlier [13].

3.3. The analysis of complex impedance spectroscopy

The complex impedance spectroscopy (CIS) [24] is a popular technique to evaluate the ac-signal impact to the sinusoidal perturbation, appropriate measured impedance data's associated with several electrical factors (grains, electrode effect and grain boundary) of the ceramic materials [5,25–28]. Fig. 7 displays a complex impedance diagram (i.e., Nyquist plot of Z' versus Z'' plot) of BNTF nanoceramic at different sets of selected temperature from room temperature to 500 °C, which leads to a succession of semicircles. The intercept extent of the smicircles on the real axis (i.e., x-axis) and its spectrum offer information on the types of electrical routes happening inside the compound and the correlation between the microstructure and arcs of said ceramics. It detected that the effect of grain boundary influence is not observed in the compound up to 200 °C.

As the increment of further temperature from a room temperature, the shape of the arc increasingly develops semicircular trend with minor movement of centre near the origin of the complex surface. On the prompt growth of temperature, an extent of slope of line losses which is turn near the Z'-axis (at above 300 °C), and hence develops semicircle may possibly representing the rise in conductivity values [29,30]. The

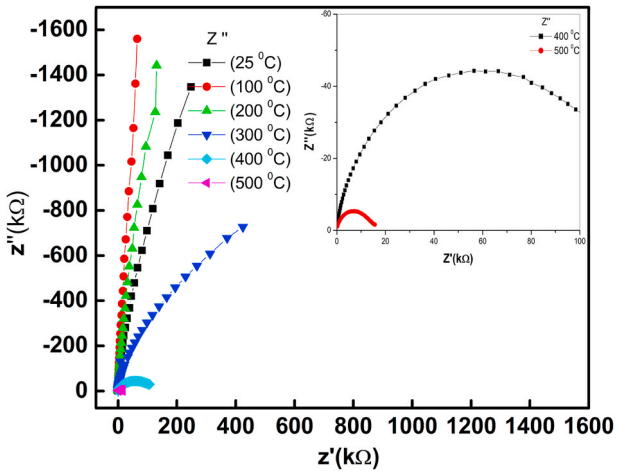

Fig. 7. Variation of complex impedance spectrum (Nyquist plots) of $Bi(Ni_{2/5}Ti_{2/5}Fe_{1/5})O_3$ nanoceramic at different selected temperatures over a wide range of frequency (25–500 kHz).

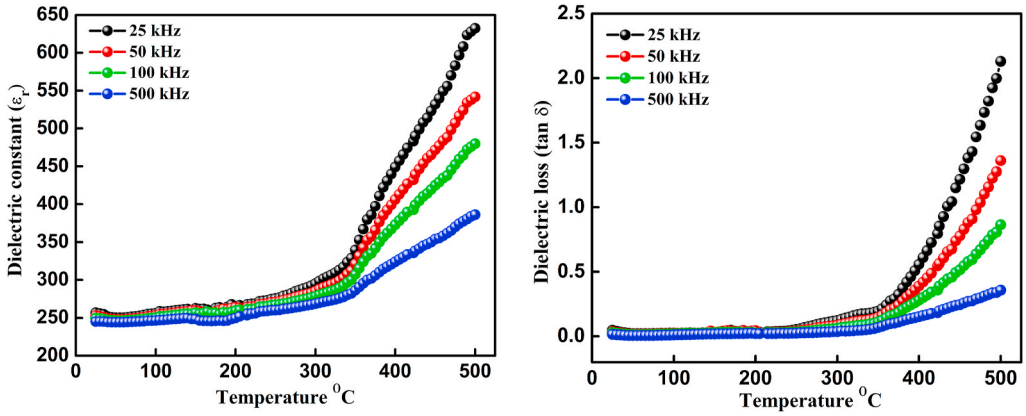

Fig. 6. (a) Variation of dielectric constant (ε_r) as a function of temperature for $Bi(Ni_{2/5}Ti_{2/5}Fe_{1/5})O_3$ nanoceramic at selected frequency
Fig. 6: (b) Variation of dielectric loss (tan δ) as a function of temperature for $Bi(Ni_{2/5}Ti_{2/5}Fe_{1/5})O_3$ nanoceramic at selected frequency.

existence of semicircular arcs above temperatures of 300 °C proposes the electrical features of the compound with a rising trend mostly because of the contributions from bulk specimens.

Furthermore, in the low-frequency zone, the magnitude of Z' decreased with the growth in temperature displays the NTCR (negative temperature coefficient of resistance) nature. This behaviour has extremely changed in the high-frequency zone displaying a total addition of the Z' spectrum beyond assured frequency. At higher-frequency, the Z' value at different temperatures coincides involving the probable space charge release [5,31]. The cut off every semi-circle on the Z' axis provides the grain boundary and bulk influences in their impedance/resistance factors. The existence of each semi-circle in the impedance plot having characteristic peak features that occurs at a particular relaxation frequency generally denoted as resonance frequency ($\omega_r = 2\pi f_r$). It could be denoted as $\omega_r RC = \omega_r \tau = 1$ and hence $f_r = 1/2\pi RC$, herein τ denotes the relaxation time. The terms of relaxation time because of the bulk effect (τ_b) has been calculated through the general relation of $\omega_r \tau_b = 1$ or, $\tau_b = 1/2\pi f_r$.

3.4. Multiferroic analysis

3.4.1. P-E loop analysis

Fig. 8 shows ferroelectric hysteresis loop of $Bi(Ni_{2/5}Ti_{2/5}Fe_{1/5})O_3$ at room temperature. The P-E loop trends were measured to estimate the ferroelectric features a few sets of applied electric field (in this study an applied electric field is between 5 and 15 kV/cm). The P-E loop analysis also proves leaky characteristic due to co-substitution of Ni and Ti into BFO. Unfortunately, it may not possible to achieve properly saturated loops of the said compound even though the applied field is beyond the breakdown voltage. At room temperature, the observed value of remnant polarization and coercive field are 0.04 μC/cm^2 and 4.11 kV/cm. The outcomes of both remnant polarization and coercive field are affected by the presence of few charged defects, thermal treatment and mechanical stresses [32,33]. Thus, said lead-free multiferroic materials may have the rich and unique benefit of innovative electrical devices over the best multiferroic system of $BiFeO_3$.

3.4.2. M − H loop analysis

In addition, Fig. 9 displays the M − H hysteresis loop of $Bi(Ni_{2/5}Ti_{2/5}Fe_{1/5})O_3$ compound and recorded at room temperature. However, the M − H loop diagram of the synthesized compound apparently reveals a saturation trend at greater magnetic field together with improved magnetic features of multi-doped BNTF. As studied compounds, the observed values of saturation magnetization (M_s), remnant magnetization (M_r) and coercivity (H_c) were found to be 0.364 emu.g^{-1}, 0.133 emu.g^{-1}, and 0.388 kOe. In addition, the existence of strong magnetic orders (at room temperature) of said compound, showing multiferroic characteristics. So far, $BiFeO_3$ [referred to as BFO] is the well-known ideal prototype of multiferroics that exhibits ferromagnetic and ferroelectric ordering simultaneously at or above room temperature. Although, the weak ferromagnetism features of BFO may limit its applications [13,34]. The magnetic characteristics of undoped BFO compounds was prepared by several methods (such as sol-gel and standard solid-state [15,16]), the attained values of M_r and M_s were about 0.0039 and 0.055 emu.g^{-1} correspondingly [35]. For the high-energy ball milling conventional technique, obtained values of H_c, M_r and M_s were approximately 1.250 kOe, 0.012 and 0.13 emu.g^{-1} [36]. Evidently, existed values are well comparable, and their results clearly reveal the enhancement of multiferroic features of nickel and titanium modified BFO compound (i.e., BNTF) [13]. These enhanced magnetization values may be occurring due to the significant doping of Ni and Ti at the Fe-site of the bismuth ferrite compound. Consequently, the strong magnetic features appeared in the BNTF compound at room temperature.

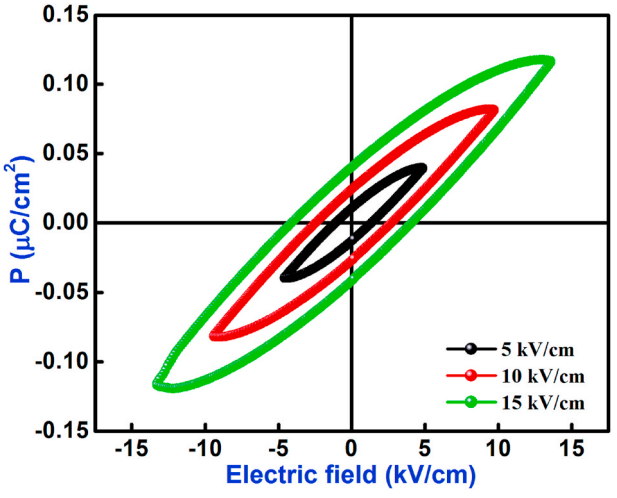

Fig. 8. Ferroelectric hysteresis loop of $Bi(Ni_{2/5}Ti_{2/5}Fe_{1/5})O_3$ compound at room temperature.

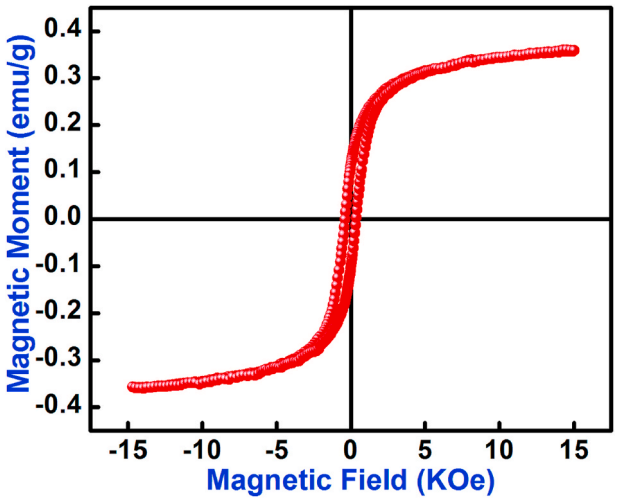

Fig. 9. Magnetic hysteresis loop of $Bi(Ni_{2/5}Ti_{2/5}Fe_{1/5})O_3$ compound at room temperature.

3.5. AC-conductivity analysis

3.5.1. Temperature dependent AC-Conductivity

For as-studied compound, the durable correlation occurs between the frequency and temperature dependent response of the electrical conductivity. The AC-conductivity (σ_{ac}) of a studied compound has been calculated and analysed by using of dielectric data with the relation of $\sigma_{ac} = \omega\, \varepsilon_0\, \varepsilon_r\, (\tan\delta)$ [13]. Fig. 10 displays the AC-conductivity variation by means of the inverse of the absolute temperature (10^3/T) at few selected sets of the frequency of BNTF compound. The ac-conductivity value is nearly constant at lower temperature region for each selected frequency. The dispersion region (strong frequency dependence) might be ascribed to the hopping of charge carriers for the arbitrary sites with flexible barrier heights. The separation as well as the magnitude of the conductivity rises with the rise in frequencies. At higher temperature regions, the conductivity plots display a higher growth with rising temperature. The variation of the σ_{ac} over an extensive operating temperature range supports thermally activated transport features of the studied series of compounds, which obey the Arrhenius equation. The trend of the curve is linear, which follows the Arrhenius behaviour: $\sigma_{ac} = \sigma_0 \exp(-E_a/k_BT)$, herein the symbols have their common notation [4]. This Arrhenius region exposes a proper Arrhenius/frequency-independent region. Hence, the variation in

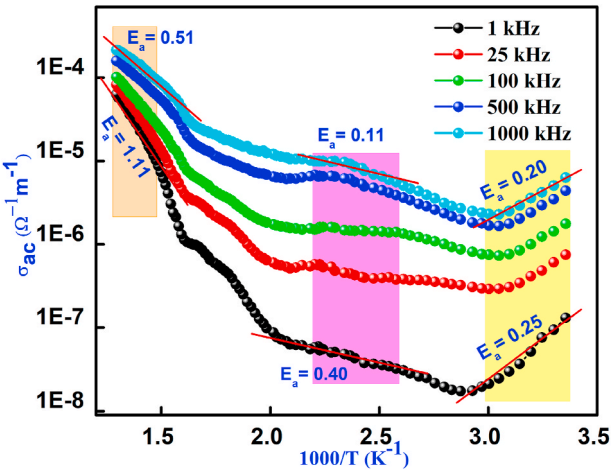

Fig. 10. Temperature dependent ac-conductivity of $Bi(Ni_{2/5}Ti_{2/5}Fe_{1/5})O_3$ compound.

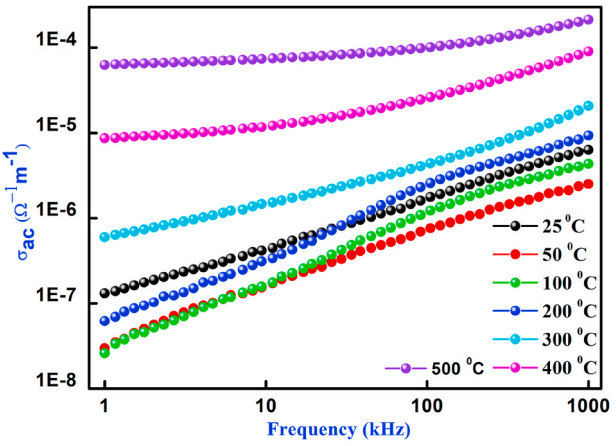

Fig. 11. Frequency dependent ac-conductivity of $Bi(Ni_{2/5}Ti_{2/5}Fe_{1/5})O_3$ compound.

conductivity (σ_{ac}) values at nominated frequency is small at the low range of temperature and much bigger at higher temperature region. The detailed explanation of conductivity and calculated activation energy of all studied sample is described in the figure itself. The activation energy has been considered to measure the slope of the curve (with linear fit) at different temperatures, especially in a low-temperature zone (yellow colour), medium temperature region (magenta colour) and high-temperature region (pink colour). The figure clearly presents that at a particular temperature the slope is changing, which might happening due to the difference in activation energy at a lower temperature (ferroelectric) and higher temperature range (paraelectric phases). The larger activation energy value may arise because of the presence of space charge polarization and oxygen vacancy (ions).

3.5.2. *Frequency dependent AC-Conductivity*

Fig. 11 depicts the variation of each conductivity nature with an extensive frequency range (1 kHz-1 MHz) at a few nominated ranges of temperature (25–500 °C) for BNTF compound. The conductivity plot clearly suggests that the studied compound displays dispersion at the low-frequency region and the conductivity value increases constantly through a rise in frequencies 5, 8]. The spectrum plot of conductivity can be fitted with the relation of well-known as Jonscher's law [14]. In the above relation, σ_α presents the frequency-independent term that offers the value of dc conductivity, β presents the frequency-dependent exponent term and its values lies in $(0 < \beta < 1)$ and the term P is a thermally activated quantity. Nevertheless, the origin of the frequency-dependent conductivity spectrum lies in the relaxation process rising due to carriers (mobile charge). However, as an effect, an increase of conductivity values with the rise in temperature and frequency proposes NTCR phenomenon (negative temperature coefficient of resistance) happened in the studied compound.

4. Conclusion

In the summary, we have successfully synthesized Ni and Ti co-doped bismuth ferrite nanoceramic [i.e., $Bi(Ni_{2/5}Ti_{2/5}Fe_{1/5})O_3$ or BNTF] through using of a conventional solid-state reaction route. We have investigated the structural, dielectric, impedance and multiferroics features of said ceramic compound. The initial structural analysis proposes that the structural variation has been detected within the significant co-substitution of nickel and titanium at the iron site of bismuth ferrite. An average crystallite size has been found to be 29 nm, which is calculated by applying Scherrer's formula. The FE-SEM image proposes that the presence of grains were aggregated in rectangular, spherical and triangular shapes. The detailed study of dielectric features illustrates both dielectric parameters (dielectric constant & loss) rise with the rise in temperature, however, the magnitude of these parameters decrease with increasing frequency. The magnitude of the bulk resistance value drops on substituting the influence of the substitution. The impedance study shows the existence of grain boundary and grains influence, which suggests NTCR behaviour in the material. The electrical conductivity of the compound studied, based on the observations of impedance parameters. The ferroelectric analysis exposes that the BNTF favours the ferroelectricity in an outstanding way which approves a non-centrosymmetric nature of the synthesized compound. The magnetic measurements at room temperature verify ferromagnetic behaviour of the BNTF sample along with slight diamagnetic influence at higher fields. Consequently, the multiferroic nature of BNTF ceramic is detected because of the synchronization of ferroelectric and ferromagnetic behaviour. Hence, the observed enhancement in the dielectric and electrical features of said BNTF nanoceramics may be used for multifunctional applications.

Data availability statement

The data that support the findings of this study are available from the corresponding author upon reasonable request.

Declaration of competing interest

The authors declare that they have no known competing financial interests or personal relationships that could have appeared to influence the work reported in this paper.

References

[1] W. Eerenstein, N.D. Mathur, J.F. Scott, Multiferroic and magnetoelectric materials, Nature 442 (2006) 759–765.
[2] S.W. Cheong, M. Mostovoy, Multiferroics: a magnetic twist for ferroelectricity, Nat. Mater. 6 (2007) 13–20.
[3] J. Hou, Y. Qu, R. Vaish, et al., Crystallographic evolution, dielectric, and piezoelectric properties of $Bi_4Ti_3O_{12}$:W/Cr ceramics, J. Am. Ceram. Soc. 93 (5) (2010) 1414–1421.
[4] N. Kumar, A. Shukla, Processing and characterization of Cd/Ti co-substituted $BiFeO_3$ nanoceramics, Int. J. Mod. Phys. B 32 (2018) 1840069. World Scientific Company.
[5] N. Kumar, A. Shukla, N. Kumar, R.N.P. Choudhary, A. Kumar, Structural, electrical and multiferroic characteristics of lead-free multiferroic: $Bi(Co_{0.5}Ti_{0.5})O_3$–$BiFeO_3$ solid solution, RSC Adv. 8 (2018) 36939–36950.
[6] H. Schmid, Multi-ferroic magnetoelectrics, Ferroelectrics 162 (1994) 317–338.
[7] C.W. Nan, M.I. Bichurin, S. Dongb, D. Viehland, Multiferroic magnetoelectric composites: historical perspective, status, and future directions, J. Appl. Phys. 103 (2008), 031101.
[8] N. Kumar, A. Shukla, N. Kumar, R.N.P. Choudhary, Effects of milling time on structural, electrical and ferroelectric features of mechanothermally synthesized multi-doped bismuth ferrite, Appl. Phys. A 126 (2020) 181.

[9] Y.P. Wang, L. Zhou, M.F. Zhang, X.Y. Chen, J.M. Liu, Z.G. Liu, Room-temperature saturated ferroelectric polarization in BiFeO3 ceramics synthesized by rapid liquid phase sintering, Appl. Phys. Lett. 84 (2004) 1731–1733.
[10] V.R. Palkar, J. John, R. Pinto, Observation of saturated polarization and dielectric anomaly in magnetoelectric $BiFeO_3$ thin films, Appl. Phys. Lett. 80 (2002) 1628.
[11] S.N.S. Reddy, D.N. Leonard, L.B. Wiggins, K.T. Jacob, Internal displacement reactions in multicomponent oxides: Part I. Line compounds with narrow homogeneity range, Metall. Mater. Trans. A Phys. Metall. Mater. Sci. 36 (2005) 2685.
[12] Y.M. Chiang III, D. Birnie, W.D. Kingery, Physical Ceramics, vol. 34, Wiley, New York, 1996.
[13] N. Kumar, A. Shukla, R.N. P Choudhary, Structural, electrical and magnetic characteristics of Ni/Ti modified $BiFeO_3$ lead free multiferroic material, J. Mater. Sci. Mater. Electron. 28 (2017) 6673–6684.
[14] N. Kumar, A. Shukla, R.N. P Choudhary, Structural, electrical and magnetic properties of (Cd, Ti) modified $BiFeO_3$, Phys. Lett. 381 (2017) 2721–2730.
[15] R. Anthony, West, Solid State Chemistry and its Applications, Wiley and Sons, 2005.
[16] B. Gerand, G. Nowogrocki, J. Guenot, M. Figlarz, Preparative Methods in Solid State Chemistry, Academic Press, 1972.
[17] V.M. Goldschmidt, Die gesetze der Krystallochemie, Naturwissenschaften 14 (1926) 477–485.
[18] B. Park, An Interactive Powder Diffraction Data Interpretations and Indexing Program Version 2.1, E. WU School of Physical Sciences, Flinders University of South Australia, SA 5042.
[19] B.D. Cullity, Elements of X-Ray Diffraction, second ed., Addison-Wesley, Publishing Company Inc., Reading, MA, USA, 1978.
[20] N. Kumar, A. Shukla, R.N. P Choudhary, Structural, dielectric, electrical and magnetic characteristics of lead-free multiferroic: $Bi(Cd_{0.5}Ti_{0.5})O_3$-$BiFeO_3$ solid solution, J. Alloys Compd. 747 (2018) 895–904.
[21] N. Kumar, A. Shukla, R.N. P Choudhary, Development of lead-free multifunctional materials $Bi(Co_{0.45}Ti_{0.45}Fe_{0.10})O_3$, Prog. Nat. Sci.: Materials International 28 (2018) 308–314.
[22] J.C. Anderson, Dielectrics, Chapman & Hall, London, 1964.
[23] L.L. Hench, J.K. West, Principles of Electronic Ceramics, John Wiley & Sons, New York, 1990.
[24] J.R. Macdonald, W.B. Johnson, Impedance Spectroscopy Theory, Experiments and Applications, John Wiley& Sons Inc, Hoboken, NJ, 2005.
[25] J.R. Macdonald, Impedance Spectroscopy Emphasizing Solid Materials and Systems, Wiley, New York, 1987.
[26] S. Sen, R.N.P. Choudhary, Impedance studies of Sr modified BaZr0. 05Ti0. 95O3 ceramics, Mater. Chem. Phys. 87 (2004) 256.
[27] S. Brahma, R.N.P. Choudhary, A.K. Thakur, AC impedance analysis of $LaLiMo_2O_8$ electroceramics, Phys. B 355 (2005) 188.
[28] C.K. Suman, K. Prasad, R.N.P. Choudhary, Complex impedance studies on tungsten-bronze electroceramic: $Pb_2Bi_3LaTi_5O_{18}$, J. Mater. Sci. 41 (2006) 369.
[29] H. Jain, C.H. Hsieh, Window effect in the analysis of frequency dependence of ionic conductivity, J. Non-Cryst. Solids 172 (1994) 1408.
[30] V. Provenzano, L.P. Boesch, V. Volterra, C.T. Moynihan, P.B. Macedo, Electrical relaxation in $Na_2O_3SiO_2$ glass, J. Am. Ceram. Soc. 55 (1972) 492–496.
[31] S. Pattanayak, B.N. Parida, P.R. Das, R.N.P. Choudhary, Impedance spectroscopy of Gd-doped $BiFeO_3$ multiferroics, Appl. Phys. A 112 (2013) 387–395.
[32] G.H. Haertling, Ferroelectric ceramics: history and technology, J. Am. Ceram. Soc. 82 (1999) 797–818.
[33] D. Damjanovic, Ferroelectric, dielectric and piezoelectric properties of ferroelectric thin films and ceramics, Rep. Prog. Phys. 61 (1998) 1267–1324.
[34] J. Wang, J.B. Neaton, H. Zheng, V. Nagarajan, S.B. Ogale, B. Liu, D. Viehland, V. Vaithyanathan, D.G. Schlom, U.V. Waghmare, N.A. Spaldin, K.M. Rabe, M. Wuttig, R. Ramesh, Epitaxial $BiFeO_3$ multiferroic thin film heterostructures, Science 299 (2003) 1719–1722.
[35] S. Sharma, V. Singh, R.K. Kotnala, R.K. Dwivedi, Comparative studies of pure $BiFeO_3$ prepared by sol–gel versus conventional solid-state-reaction method, J. Mater. Sci. Mater. Electron. 25 (2014) 1915–1921.
[36] D. Maurya, H. Thota, K.S. Nalwa, A. Garg, $BiFeO_3$ ceramics synthesized by mechanical activation assisted versus conventional solid-state-reaction process: a comparative study, J. Alloys Compd. 4 (2009) 477–780.